The Kinetics of Tetramethylethene Ozonolysis: Decomposition of the Primary Ozonide and Subsequent Product Formation in the Condensed Phase

Scott A. Epstein and Neil M. Donahue*

Center for Atmospheric Particle Studies, Carnegie Mellon University, Pittsburgh, Pennsylvania 15213

Received: August 28, 2008; Revised Manuscript Received: October 31, 2008

We report data from real-time FTIR temperature programmed reaction spectroscopy on a cryogenic zinc selenide window revealing the intermediates from ozonation of 2,3-dimethyl-2-butene (TME). We have found convincing evidence of a 1,2,3-trioxolane (the primary ozonide, POZ), which decomposes at 185 K to yield a 1,2,4-trioxolane product (the secondary ozonide, SOZ). Computational infrared spectra confirmed the presence of the POZ and SOZ. The barrier height for POZ decomposition, determined experimentally, was found to be 13.8 ± 1.0 kcal mol^{-1}, and the *A* factor calculated with RRKM theory based on density functional reactant and transition state frequencies was found to be 4.16×10^{13} s^{-1}. The TME SOZ has not previously been observed without the presence of a polyethylene surface. SOZ formation kinetics from the reaction of the POZ decomposition products along with the competing reaction pathways were examined with computational chemistry calculations using DFT. These calculations confirm our experimental observation of SOZ formation.

Introduction

Ozonolysis is the most important sink for many unsaturated gases and condensed-phase species in the atmosphere.[1,2] In addition, ozonolysis is an important source of radicals.[3,4] Because ozonolysis products often have lower vapor pressures than the reactants, ozonolysis is also a major source of organic particulate matter.[5,6] Ozone reacts with atmospheric particulate matter as well, making ozonolysis an important particle aging process.[7,8]

Ozonolysis is a multistep process with several intermediates and a wide range of products. The widely accepted mechanistic model was developed by Criegee[9−11] in the early 1950s. The Criegee mechanism involves the formation of a short-lived 1,2,3-trioxolane (primary ozonide, POZ) from the reaction of an alkene and ozone. The POZ decomposes into a carbonyl-*O*-oxide (COO) known as the Criegee intermediate: the COO electronic structure combines zwitterionic and biradical character.[12] Along with the COO, POZ decomposition produces an aldehyde or ketone (depending on the degree of substitution of the reactant alkene) which is referred to as the carbonyl coproduct (CCP). This decomposition is first order in POZ concentration and the decomposition products are formed immediately.[10,13] The POZ formed from an unsymmetrical olefin can cleave along two different sets of O−O bonds, leading to multiple carbonyl coproducts and carbonyl-*O*-oxides. The subsequent fate of the COO and CCP is sometimes uncertain as it depends on their reactivity and environment.

Our objective is to study the earliest stages of ozonolysis—the formation and subsequent decomposition of the POZ—via temperature controlled reaction spectroscopy (TPRS) on cryogenically cooled IR-transparent windows with real-time FTIR spectroscopy. By constraining the POZ decomposition barrier heights experimentally, we plan to directly probe the factors controlling selectivity in the ozonolysis mechanism: here we describe initial experiments on a symmetric system, 2,3-dimethyl-2-butene (tetramethylethene, TME) as the first step in this process. The advantages of TME are 2-fold: First, TME is one of the most widely studied ozonolysis reagents,[3,14−22] and second, because it is symmetric, we expect it to produce only one POZ, one CCP, and one COO. In the future, this method will be extended to study the decomposition of POZ species formed from the ozonolysis of disubstituted, trisubstituted, tetrasubstituted, endocyclic, and exocyclic alkenes.

The COO and CCP formed from the ozonation of TME in the liquid phase are acetone-*O*-oxide and acetone, respectively. The acetone-*O*-oxide produces a wide distribution of products (Figure 1). It is believed that dimerization of the COO will produce a diperoxide ring (DiP).[10,19,22,23] Trimers (TiP) and polymers from the COO have also been observed.[22,24−27] It has also been suggested that isomerization of the COO will lead to a vinyl hydroperoxide (VHP).[25,28,29] The VHP can isomerize into hydroxyacetone, which can react with another COO to form a 6-member ring (COOHA). However, in the gas phase, the VHP is thought to decompose into an alkoxy radical and the OH radical. This is the major pathway for OH radical formation from ozonolysis in the gas phase.[30−33] There is also some evidence of the cyclization of the COO leading to a dioxirane (DiO)[19,34] and then an epoxide,[19] but this mechanism is uncertain. The VHP and DiO pathways are both unimolecular pathways for the COO, and so their relative importance depends primarily on the relative barrier heights of the pathways. It appears that these barrier heights depend on the degree of substitution and the stereochemistry of the COO: if the COO is syn to an R group containing a proton, the VHP pathway is favored, while if it is anti to an R group, the DiO pathway is favored.[30] The reactant concentrations, the presence of solvents, and the reaction temperature all affect the final product distribution.[10,19,26]

Until 1985, the TME secondary ozonide (SOZ) had not been observed. The belief was that ozonolysis of TME did not produce a SOZ because decomposition of the POZ yields a ketonic CCP as opposed to the aldehyde that is formed from nontetrasubstituted olefins. The ketonic CCP (acetone) formed by POZ decomposition was assumed to be unreactive toward

* Author to whom correspondence should be addressed. Mailing address: Center for Atmospheric Particle Studies, Carnegie Mellon University, B204 Doherty Hall, 5000 Forbes Ave., Pittsburgh, PA 15213 E-mail: nmd@cmu.edu. Phone: (412)-268-4415. Fax: (412)-268-7139.

10.1021/jp807682y CCC: $40.75
Published on Web 12/04/2008

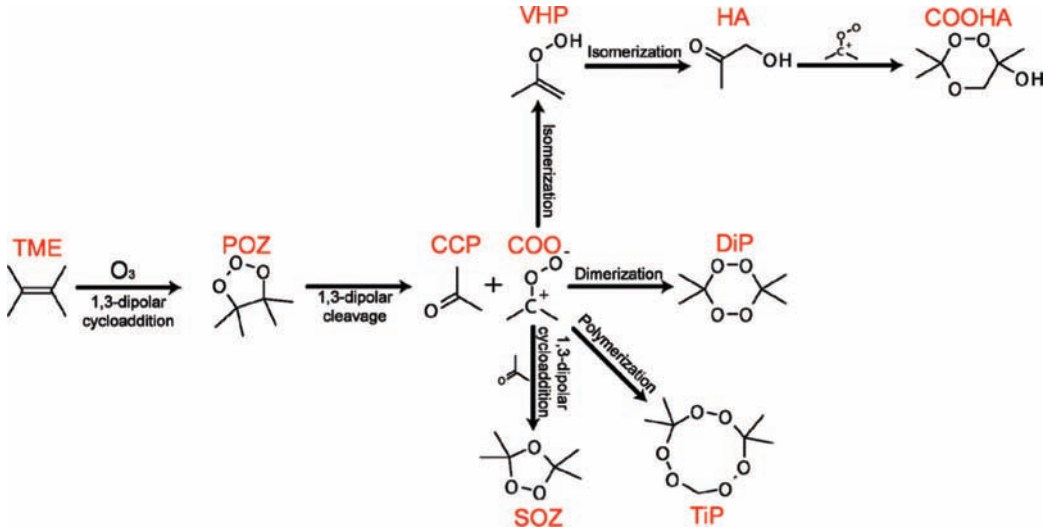

Figure 1. A summary of the TME ozonolysis reaction in the condensed phase.

the COO.[10] In addition, Criegee suggested that isomerization of the COO dominates the SOZ formation pathway.[35] However, in 1985, Griesbaum et al.[22,36] discovered convincing evidence of the TME SOZ by ozonation of TME on a polyethylene powder. They found that the TME SOZ was stable even at temperatures of 353 K. It is hypothesized that ozonolysis on a substrate such as the polyethylene powder or silica gel[37] helps to immobilize the decomposition products at their point of origin, thus encouraging the formation of secondary ozonides from tetrasubstituted alkenes.[19,22] This suggests that the previous inability to form the TME SOZ was not due to the reactivity of the CCP.[19]

To study the POZ and its decomposition kinetics and products, one can observe the ozonolysis of condensed alkenes on a cryogenic surface. The POZ has been observed on a cold surface using various methods, including microwave spectroscopy,[38,39] nuclear magnetic resonance,[13,38,40,41] and infrared spectroscopy.[17,38,42−45] We have designed an apparatus to perform kinetic studies of primary ozonide decomposition with real-time Fourier transform infrared spectroscopy (FTIR).

Experimental Details

Materials. Ozone is produced from a corona discharge ozone generator [Pacific Ozone Technologies]. The ozone generator produces an ozone/oxygen mixture of an unknown composition. In a typical experiment, approximately 1 L at 8 psig of this mixture is sprayed onto the cryogenic surface. We have used 2,3-dimethyl-2-butene (TME) obtained from Aldrich at 99+% purity as the reagent alkene, without further purification.

Experimental Methods. We constructed an apparatus to perform TPRS of ozonolysis on a cryogenic surface. This surface consists of a set of zinc selenide (ZnSe) windows that are cooled by conduction with a copper block in contact with boiling liquid nitrogen (LN_2). ZnSe was chosen as the window material because its infrared transmission properties allow light in our desired frequency range (500 to 3500 cm^{-1}) to pass through virtually unobstructed. In addition, ZnSe windows do not fog with humidity and are not reactive with TME and ozone. It is important to note that the windows do not significantly participate in the chemistry but are merely a surface to condense the reagents on and control their temperature. The volume of TME alone provides a surface film on the order of 10,000 molecular layers thick therefore negating any effects that the surface might have on the first few molecular layers.

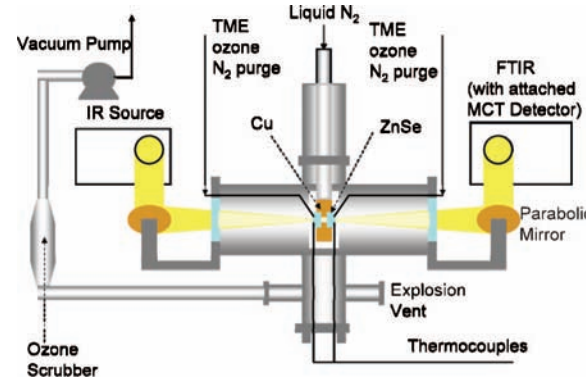

Figure 2. Apparatus schematic consisting of a liquid nitrogen coldfinger in thermal contact with two ZnSe windows. The reactants are added through two injection ports that terminate right above the window surfaces.

An Oriel MIR8000 modular Fourier transform infrared (FTIR) spectrometer is used to monitor the reaction at a resolution of 2 cm^{-1}. A LN_2 cooled mercury cadmium telluride (MCT) detector [Judson Technologies] and an infrared source [Thermo Oriel] are used along with the FTIR spectrometer. A schematic of the apparatus is presented in Figure 2. In an experiment, the reactants are sprayed onto the cryogenic windows, which are cooled to 90−100 K. A consistent dry nitrogen purge is passed over the windows and pumped out with a rotary vane 2-stage vacuum pump. The purge is minimal enough to permit pressures as low as 0.1 torr (13.3 Pa) to be achieved. Operating at a low pressure is advantageous because conductive and convective heat transfer to the window surface is minimized. In addition, constant pumping ensures that evaporated species are swept out of the reaction chamber and are not detected by the FTIR. The nitrogen purge also helps keep the surface free of contaminates such as carbon dioxide and water.

The reactant and product concentrations on the surface are monitored continuously as the surface is warmed. The temperature of the reactant and products are monitored every second with two Omega type "K" thermocouples equipped with cold junction compensation which are mounted on the ZnSe windows at the closest point possible to the reactant mixture. The temperature difference of the two opposing windows during heating is less than 1 K. To warm the surface, either a resistively heated rod is inserted into the LN_2 reservoir of the coldfinger, or air heated to 473 K is passed through the LN_2 reservoir. With

these heating methods, it is possible to achieve a heating rate between 0.04 and 0.4 K s^{-1}. Slow heating rates lead to better temperature resolution, but are disadvantageous because of the additional time molecules are given to evaporate from the surface even at low temperatures.

Calculation of the absorption spectrum from the measured transmission spectrum is complicated by the dependence on the background transmission spectrum with temperature. At each temperature, asymmetrical least squares smoothing[46] of the spectra was used to estimate a reasonable background. This technique weights negative deviations in the transmission spectrum (indicative of chemical species) to a lesser extent than any positive deviations in the transmission to create a background spectrum. The absorption spectrum was calculated by taking the negative $\log_{10}$ of the ratio of the transmission spectrum and the background spectrum.

The areas of the absorption peaks representing the POZ were calculated as a function of temperature. The absorption peak area is proportional to the concentration of the species that it represents.[47] A linear baseline was calculated from the absorption spectrum directly under a peak. Integration of each absorption peak above the linear baseline yielded the absorption peak area. Absorption peak area as a function of temperature was calculated for several peaks at a temperature resolution ranging from 0.5 to 3 K.

We use the Redhead equation[48] to model the reaction kinetics of a system in which the temperature is constantly changing. The Redhead equation can be derived for a reacting system in which the activation energy (E_a) is analogous to the desorption energy for temperature programmed desorption (TPD) and the reaction pre-exponential factor (A) is analogous to the desorption pre-exponential factor for TPD (see Supporting Information). β is the heating rate of the experiment in units of (K s^{-1}), R is the ideal gas constant, and T_P is the peak reaction temperature defined as the temperature in which the sigmoidal concentration curve has an inflection point.

$$\ln\left(\frac{\beta}{T_p}\right) = \ln\left(\frac{AR}{E_a}\right) - \frac{E_a}{RT_p} \quad (1)$$

The POZ peak-area curve relates POZ concentration to temperature, and a minimum in its derivative marks the peak reaction temperature. The activation energy of POZ decomposition can then be calculated from the slope of a plot of $\ln(\beta/T_p)$ vs $1/T_p$. The instrument we employed does not allow us to constrain the A factor with the plotted intercept due to the limited range of peak temperatures and noise associated with background fluctuations; small deviations in the slope lead to large changes in the A factor. Therefore, the A factor was determined using computational methods.

Gaussian 03[49] was used to calculate the vibrational frequencies of the TME POZ and various transition states. Density functional theory (DFT) using the hybrid function B3LYP and the 6-31G(d) basis set was used with microcanonical RRKM theory[50] to predict the pre-exponential factor *a priori* as Chuong, Zhang, and Donahue[51] employed for the cyclohexene primary ozonide. The suggested correction factor[52] of 0.9613 was used to scale the frequencies.

Hazards. Because ozone and primary ozonides are potentially explosive, care was taken to use the least amount of reactants possible. In addition, all metal parts in thermal contact with LN_2 were insulated to avoid the inadvertent collection of ozone inside the pressure vessel.

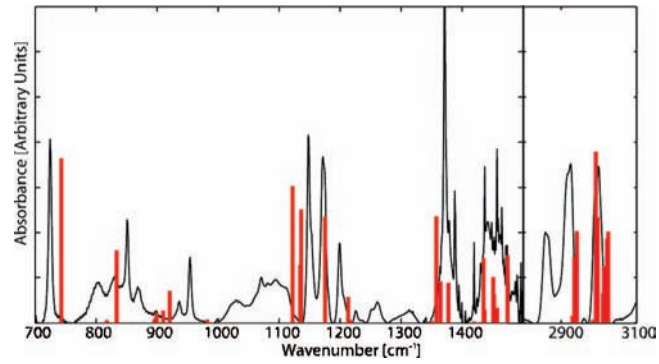

Figure 3. Comparison between the TME POZ spectrum predicted by Gaussian 03 at the DFT 6-311G++(2d,2p) level (red) and the baseline corrected spectra measured at 174 K for a representative TME ozonolysis experiment (black). Notice general agreement between both the intensity and the frequency of the predicted and measured peaks indicating the presence of the POZ.

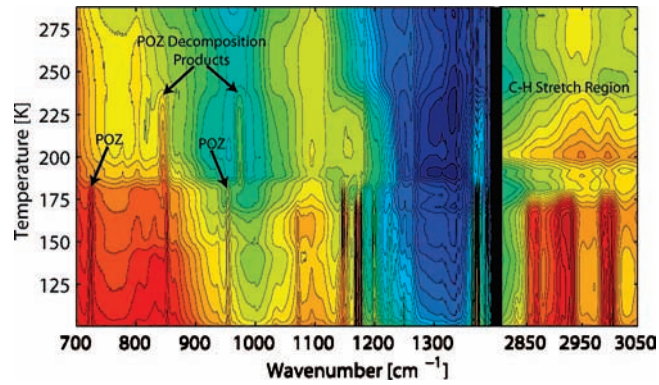

Figure 4. Contour plot of a single experiment in which TME and O_3 were reacted on ZnSe windows at 100 K and warmed at a rate of approximately 0.25 K/s. Within the Z axis, warmer colors indicate low transmission while colder colors indicate higher transmission. Strongly sloped contours indicate peaks.

Results

Characteristic peaks for the POZ were identified by comparing spectra for experiments in which TME was reacted with ozone and to experiments in which solely TME was added and desorbed. In addition, Gaussian 03 was used to predict an infrared spectrum of the POZ with DFT using the B3LYP hybrid functional and the 6-311G++(2d,2p) basis set after it was proved to produce an accurate spectrum for TME (see Supporting Information). Rough agreement was found between the spectrum predicted by Gaussian and the product spectra taken at temperatures below approximately 185 K, see Figure 3. Three strong POZ peaks were found at 685, 725, and 852 cm^{-1}. Heicklen et al.[17] found corresponding peaks at 682, 721, and 852 cm^{-1} at 88 K in a neat film. Samuni and Hass[20] also identified POZ peaks experimentally in an argon matrix at 37 K occurring at 691, 729, and 854 cm^{-1}. These POZ peaks are merely a partial list, and many other significant POZ peaks are present, but interference from possible TME reagent peaks complicates their analysis.

In all experiments, the absorption peaks that we identified as the POZ decreased sharply as the temperature reached approximately 185 K, indicating decomposition. Three additional product peaks were formed concurrently with POZ decomposition at frequencies of 845, 975, and 1700 cm^{-1}. Figure 4 captures the results of an entire experiment with an average heating rate of 0.27 K s^{-1} in a single contour plot. We know that the POZ decomposition product peaks evident at 845 and

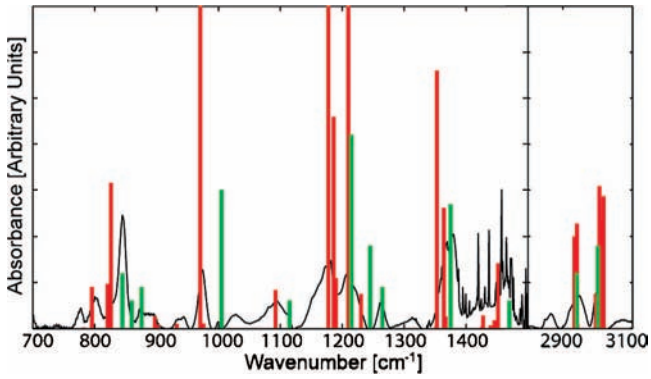

Figure 5. Comparison between the TME SOZ spectrum predicted by Gaussian at the B3LYP 6-311G+(2d,2p) level (red), the spectrum obtained by ozonolysis of TME on polyethylene which was assumed to be the TME SOZ[22] (green), and the baseline corrected spectra measured at 210 K for a representative TME ozonolysis experiment (black) from this work. Notice general agreement between all sets of data indicating the presence of the TME SOZ.

975 cm^{-1} form directly after the POZ decomposes and cannot be confused with the reactant peaks because TME and ozone evaporate at significantly lower temperatures.

The infrared spectrum of the TME SOZ was calculated with Gaussian 03 using DFT B3LYP 6-311G+(2d,2p) and compared to a spectrum of the POZ decomposition products. The correlation between the calculated spectrum and the POZ decomposition products suggests the presence of the TME SOZ (see Figure 5). Furthermore, we can also rule out the presence of the other possible POZ decomposition products observed by other researchers. Significant formation of the diperoxide does not occur in these experiments. The computed spectrum of the diperoxide fails to predict the strong decomposition product peaks at 975, 1094, 1208 cm^{-1}, which are accurately modeled by the SOZ predicted spectrum. Also, the computed diperoxide spectrum has a strong feature at 913 cm^{-1} whereas the experimental spectrum does not have any significant peaks between 880 and 960 cm^{-1}. Significant formation of the COOHA can also be ruled out due to the absence of a strong peak in the 1050 cm^{-1} range, which is characteristic of primary alcohols.[53] In addition, there is little agreement between the measured spectrum and the infrared spectral data obtained from Story and Burgess[28] in which ozonolysis of TME produced the COOHA. Finally, a computational spectrum of the epoxide does not have any features around 845 or 975 cm^{-1}, thus eliminating it as a possible product.

While it is not possible to conclusively say that the two strong peaks at 845 and 975 cm^{-1} are from the SOZ, all of our evidence suggests that the SOZ was formed. An additional product peak is exhibited at 1700 cm^{-1} at temperatures above 185 K, which we hypothesize to be the carbonyl stretch from the carbonyl coproduct (acetone).

In order to determine the peak reaction temperature for the POZ decomposition, we calculate the inflection point in the absorption peak area curve. For evaporating species, the inflection point temperature corresponds to the peak desorption temperature. Peak reaction temperatures for species that are forming on the window can be calculated with the same methodology.

The concentration as a function of temperature for several intermediates is plotted in Figure 6 for a TME ozonolysis experiment with an average heating rate of 0.3 K/s. The plot shows peak areas after TME and an excess of ozone were condensed on the window. The three identified POZ peaks at

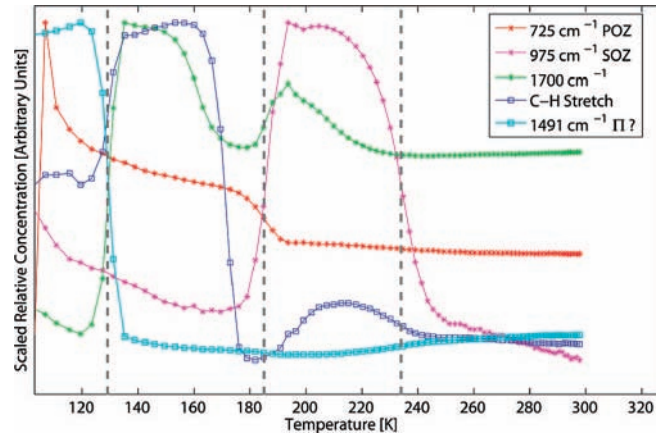

Figure 6. Absorption peak area as a function of temperature for an identified POZ peak, an identified POZ decomposition product peak (labeled SOZ), a peak occurring in the carbonyl stretch region for acetone, and a peak possibly indicating a π-complex. Notice that POZ concentration exhibits a sharp decrease as the POZ decomposition products and carbonyl stretch peak areas are increasing indicating decomposition of the POZ.

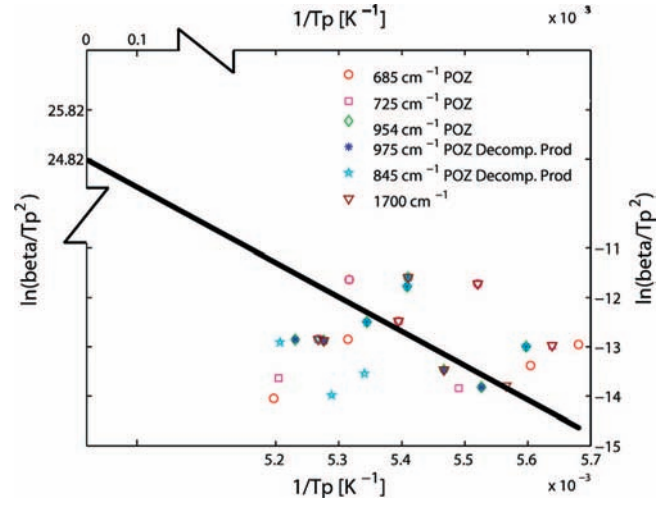

Figure 7. A Redhead plot of a set of 8 experiments and each of their relevant POZ decomposition peaks. Notice that there is no trend in peak reaction temperature as the decomposition peak frequency is varied. The theoretically determined A-factor of 4.17×10^{13} s^{-1} was used to iteratively force the y-intercept.

685, 725, and 954 cm^{-1} are used to monitor the POZ concentration. All POZ peaks exhibit the same trend in concentration. For simplicity, only the 725 cm^{-1} peak is shown in Figure 6. A more complete plot is shown in the Supporting Information. All three peaks exhibit sharp decreases at 185 $\pm$ 2 K, the peak reaction temperature for this experiment. The peaks indicative of the POZ decomposition products at 975 and 845 cm^{-1} increase sharply as the POZ peaks shrink. The peak reaction temperature for the formation of the POZ decomposition products is 186.4 $\pm$ 0.5 K, which is coincident with the peak reaction temperature obtained from the decomposition of the POZ. At a similar peak reaction temperature of 186.2 $\pm$ 0.5 K, a peak centered at 1700 cm^{-1} grows abruptly: this is most likely due to the acetone coproduct. The POZ decomposition products appear to stay relatively stable until they finally desorb with a peak desorption temperature of 233.7 $\pm$ 0.5 K. Another noteworthy region of product disappearance occurs at a peak reaction/desorption temperature of 129.3 $\pm$ 0.5 K, where two strong product peaks centered at 2831 cm^{-1} and 1491 cm^{-1} decrease drastically. We hypothesize that these peaks are due

TABLE 1: Summary of Kinetic Parameters Calculated within This Work[a]

reaction	method	*A*	E_a, kcal/mol
POZ to CCP + COO	experimental		13.8 ± 1.0
	DFT B3LYP 6-31G d	4.16E13 s^{-1}	14.4
COO to VHP	DFT B3LYP 6-31G 2d2p	8.4E12 s^{-1}	14.8
COO to diperoxide	DFT B3LYP 6-31G 2d2p	4.42E−16 cm^3 s^{-1} $molec^{-1}$	13.3
CCP + COO to SOZ	DFT B3LYP 6-31G 2d2p	2.43E−16 cm^3 s^{-1} $molec^{-1}$	3.0

[a] RRKM theory used for unimolecular reactions, transition state theory used for bimolecular reactions. Energies and vibrational frequencies used to calculate *A* and E_a for COO to VHP reaction are from ref 21. DFT B3LYP 6-31G d was used in Chuong et al.[51] to model cyclohexene primary ozonide decomposition. DFT B3LYP 6-31G 2d2p was used to model various steps of the TME ozonolysis reaction in refs 21, 33, 55, and 56. All transition states were optimized with QST2.[57]

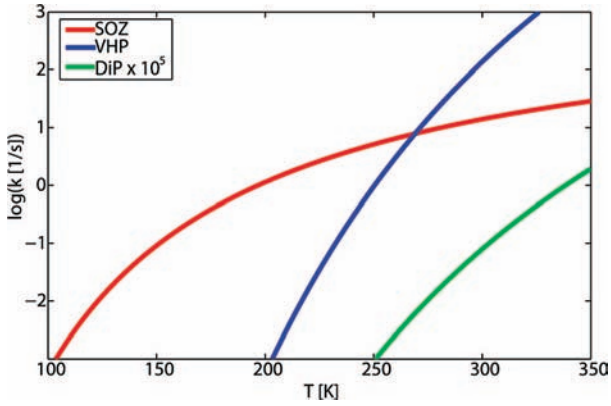

Figure 8. Theoretically calculated rate constants as a function of temperature. The VHP becomes the favored route at temperatures above 270 K. A COO and CCP concentration of 8.9×10^{18} molecules/cm^3 was used to calculate the rate of reaction.

to a π-complex. Both Hull et al.[17] and Mile and Morris[43] have found evidence of π-complexes. These complexes are known to be only stable to temperatures up to 133 K.[10]

The curve based on the C−H stretch region (2835−3014 cm^{-1}) in Figure 6 shows a peak temperature at 171.3 ± 0.5 K, which is significantly below the POZ peak reaction temperature which can be attributed to the desorption of excess TME. This signal also exhibits a second desorption with a peak temperature of 230.9 ± 0.5 K, which is most likely due to desorption of the POZ decomposition products.

Peak reaction temperatures were calculated for a series of eight experiments with heating rates ranging from 0.07 to 0.31 K/s. $\ln(\beta/T_p^2)$ as a function of the inverse peak temperature for all peaks which indicate POZ decomposition are plotted in Figure 7. We used the theoretical pre-exponential factor (calculated with RRKM theory and DFT B3LYP 6-31G d) to constrain the intercept and iteratively determine the activation energy of the reaction using equation 1.

With this analysis, the activation energy for POZ decomposition is 13.8 ± 1.0 kcal mol^{-1}. Misestimating the theoretical pre-exponential factor by a factor of 10 will only induce a 6% change in the calculated activation energy. We also calculated the activation energy using DFT B3LYP 6-31G d as used by Atkinson and Aschmann[54] and Gutbrod et al.[55] The computational (zero-point corrected) barrier height of 14.4 kcal mol^{-1} agrees well with the experimentally determined activation energy.

Calculation of the peak reaction and desorption temperatures is a very robust process. With all curves shown in Figure 6, there may be regions of erratic behavior due to interference from neighboring peaks as the temperature is varied, but the large sigmoidal reaction or desorption region is very well-defined; the area of reaction or desorption trumps out all other variations. In order to test the uncertainty in the peak temperatures resulting from the asymmetric least squares background fit, we calculated peak temperatures using background spectra determined with an entire range of fitting parameters including obviously poor fits. The average peak temperature is constant within 0.25 K, and the standard deviation is 1.8 K. A 1.8 K bias in the peak reaction temperatures will change the final barrier height determination by 1%. Moreover, experimental uncertainties due to calculation of the background spectrum estimation do not significantly contribute to uncertainties in the barrier height.

The branching of possible COO reaction pathways was also examined theoretically with DFT B3LYP 6-31G 2d2p following previous treatments.[21,33,55,56] All transition states were optimized with QST2 constrained saddle-point optimization.[57] The results of these calculations are detailed in Figure 7 and Table 1. Figure 7 shows the rate constants as a function of temperature for three of the possible COO reaction pathways. Table 1 summarizes these results in tabular form. In order to compare the unimolecular rate constant for VHP formation to the bimolecular rate constants for diperoxide formation and SOZ formation, we calculated the CCP and COO concentrations based on estimates of the TME and O_3 concentrations. Although Figure 7 should not be interpreted quantitatively, the slight dependence of CCP and COO concentrations on the calculated rate constants permits a qualitative interpretation. Figure 8 indicates that formation of the SOZ is considerably faster than the DiP and VHP route at temperatures lower than 270 K. The VHP route is favored at all temperatures above 270 K.

Discussion

The barrier height for TME POZ decomposition obtained experimentally with a Redhead analysis compares well to the theoretically predicted value.

We see clear evidence for SOZ formation without an obvious role of a catalytic surface. According to our theoretical calculations of the possible COO decomposition pathways, formation of the SOZ is favored at all temperatures below approximately 270 K. We observe POZ decomposition at 185 K followed by immediate SOZ formation, and our calculations confirm that SOZ formation is expected under these conditions. Our calculations show that acetone is reactive toward the acetone-*O*-oxide. However, the VHP route is favored at temperatures above 270 K; consequently, room-temperature experiments may fail to cause SOZ formation while our low-temperature experiments do. This is part of a broad pattern of reactivity: high-barrier, high-entropy pathways are favored at high temperature, whereas low-barrier, low-entropy pathways become competitive at low temperature. Unimolecular reactions, such as the VHP formation under consideration here, have a high barrier and sample that barrier at the vibrational frequency (3×10^{13} Hz). In contrast, SOZ formation has a low barrier and low entropy because it requires a collision (about 3×10^{12} Hz with the solvent in the condensed phase) and because it is a cyclization reaction (the

appropriate TS geometry occurs in less than 1 in 10,000 collisions). Therefore, if it is warm enough, isomerization to the VHP will prevail, but below 270 K (in this case), SOZ formation is dominant.

Other low-temperature experiments described in the literature do not report SOZ formation.[17,20] We propose several reasons for these differences. While all of our experiments were performed in an environment as dry as possible, the presence of water or other unknown contaminants could change the resulting products. In addition, in other experiments, it is also possible for solvent effects to direct the mechanism to favor a certain product. Another explanation is that the carbonyl-*O*-oxide and acetone evaporate from the window immediately after they are formed. However, a thin film which is adsorbed onto the window surface remains and then reacts to form the SOZ. We know that TME ozonolysis on a surface can lead to the formation of the SOZ. Additionally, the continuous purge of the reaction vessel could allow us to detect the SOZ more clearly than in previous experiments performed on IR windows by reducing the likelihood that gas-phase products will recondense on the window.

Conclusion

We have developed an instrument to perform temperature programmed reaction spectroscopy of ozonolysis reactions on a cryogenic IR-transparent surface. With this instrument, we can identify the TME primary ozonide, measure its subsequent decomposition, and observe the formation of a secondary ozonide product. We are also able to experimentally determine the activation energy of POZ decomposition. DFT calculations are consistent with the experimental values. They support the activation energy determination by constraining the decomposition pre-exponential factor, and also predict barrier heights consistent with the experiment. In addition, calculated rate constants for the loss kinetics of the carbonyl-*O*-oxide formed upon POZ decomposition confirm that SOZ formation should be favored at the low temperatures of these experiments. Our experimental and computational results are thus fully self-consistent.

Acknowledgment. This work was supported by Grant CHE-0717532 from the National Science Foundation. We thank Andy Gellman for providing the coldfinger used in these experiments.

Supporting Information Available: A derivation of the Redhead equation for reacting species, a verification of the level of theory used to predict the POZ and SOZ spectra, and a more complete version of Figure 6. This material is available free of charge via the Internet at http://pubs.acs.org.

References and Notes

(1) Atkinson, R.; Carter, W. P. L. Kinetics and Mechanisms of the Gas-Phase Reactions of Ozone with Organic Compounds under Atmospheric Conditions. *Chem. Rev.* **1984**, *84*, 437–470.

(2) Grosjean, D. Gas-phase reaction of ozone with 2-methl-2-butene: dicarbonyl formation from Criegee biradicals. *Environ. Sci. Technol.* **1990**, *24* (9), 1428.

(3) Donahue, N. M.; Kroll, J. H.; Anderson, J. G.; Demerjian, K. L. Direct observation of OH production from the ozonolysis of olefins. *Geophys. Res. Lett.* **1998**, *25* (1), 59–62.

(4) Aschmann, S. M.; Arey, J.; Atkinson, R. OH radical formation from the gas-phase reactions of O3 with a series of terpenes. *Atmos. Environ.* **2002**, *36* (27), 4347–4355.

(5) Donahue, N. M.; Hartz, K. E. H.; Chuong, B.; Presto, A. A.; Stanier, C. O.; Rosenhorn, T.; Robinson, A. L.; Pandis, S. N. Critical factors determining the variation in SOA yields from terpene ozonolysis: A combined experimental and computational study. *Faraday Discuss.* **2005**, *130*, 295–309.

(6) Pandis, S.; Harley, R.; Cass, G.; Seinfeld, J. Secondary organic aerosol formation and transport. *Atmos. Environ.* **1992**, *26A*, 2269–2282.

(7) Rudich, Y. Laboratory Perspectives on the Chemical Transformations of Organic Matter in Atmospheric Particles. *Chem. Rev.* **2003**, *103* (12), 5097–5124.

(8) Katrib, Y.; Biskos, G.; Buseck, P. R.; Davidovits, P.; Jayne, J. T.; Mochida, M.; Wise, M. E.; Worsnop, D. R.; Martin, S. T. Ozonolysis of Mixed Oleic-Acid/Stearic-Acid Particles: Reaction Kinetics and Chemical Morphology. *J. Phys. Chem. A* **2005**, *109* (48), 10910–10919.

(9) Criegee, R. Uber Den Verlauf Der Ozonspaltung 0.3. *Justus Liebigs Ann. Chem.* **1953**, *583* (1), 1–2.

(10) Bailey, P. S. *Ozonation in Organic Chemistry*; Academic Press: New York, 1978; Vol. I.

(11) Criegee, R. Mechanism of Ozonolysis. *Angew. Chem., Int. Ed. Engl.* **1975**, *14* (11), 745–752.

(12) Bunnelle, W. Preparation, Properties, and Reactions of Carbonyl Oxides. *Chem. Rev.* **1991**, *91*, 335–362.

(13) Greenwood, F. L.; Durham, L. J. Ozonolysis. XI Kinetic studies on the conversion of the molozonide to ozonolysis products. *J. Org. Chem.* **1969**, *34* (11), 3363–3366.

(14) Martinez, R. I.; Herron, J. T. Stopped-Flow Studies of the Mechanisms of Ozone-Alkene Reactions in the Gas Phase: Tetramethylethylene. *J. Phys. Chem.* **1987**, *91*, 946–953.

(15) Lambe, A.; Zhang, J.; Donahue, N. M. Controlled OH radical production via Ozone-Alkene reactions for use in aerosol aging studies. *Environ. Sci. Technol.* **2007**, *41* (7), 2357.

(16) Niki, H.; Maker, P. D.; Savage, C. M.; Breitenbach, L. P.; Hurley, M. D. FTIR Spectroscopic Study of the Mechanism for the Gas-Phase Reaction between Ozone and Tetramethylethylene. *J. Phys. Chem.* **1987**, *91*, 941–946.

(17) Hull, L. A.; Hisatsune, I. C.; Heicklen, J. Low-Temperature Infrared Studies of Simple Alkene-Ozone Reactions. *J. Am. Chem. Soc.* **1972**, *94* (14), 4856–4864.

(18) Lockley, J. E.; Ebdon, J. R.; Rimmer, S.; Tabner, B. J. Polymerization of methyl methacrylate initiated by ozonates of tetramethylethene. *Polymer* **2001**, *42* (5), 1797–1807.

(19) Murray, R. W.; Kong, W.; Rajadhyaksha, S. N. The ozonolysis of tetramethylethylene. Concentration and temperature effects. *J. Org. Chem.* **1993**, *58* (2), 315–321.

(20) Samuni, U.; Haas, Y.; Fajgar, R.; Pola, J. Matrix effects in the low-temperature ozonation of ethylene, tetramethylethylene and 1-hexene. *J. Mol. Struct.* **1998**, *449* (2−3), 177–201.

(21) Olzmann, M.; Kraka, E.; Cremer, D.; Gutbrod, R.; Andersson, S. Energetics, kinetics, and product distributions of the reactions of ozone with ethene and 2,3-dimethyl-2-butene. *J. Phys. Chem. A* **1997**, *101* (49), 9421–9429.

(22) Griesbaum, K.; Volpp, W.; Greinert, R.; Greunig, H. J.; Schmid, J.; Henke, H. Ozonolysis of tetrasubstituted ethylenes, cycloolefins, and conjugated dienes on polyethylene. *J. Org. Chem.* **1989**, *54* (2), 383–389.

(23) Criegee, R.; Blust, G.; Zinke, H. Eine Neuartige Synthese Von Ozoniden. *Chem. Ber.-Recl.* **1954**, *87* (5), 766–768.

(24) Criegee, R.; Lohaus, G. *Justus Liebigs Ann. Chem.* **1953**, *583*, 6.

(25) Milas, N. A.; Belic, I. *Vestn. Slov. Kem. Drus.* **1963**, *10*, 37.

(26) Barton, M.; Ebdon, J. R.; Foster, A. B.; Rimmer, S. Ozonolysis of tetramethylethylene: Characterization of cyclic and open-chain oligoperoxidic products. *J. Org. Chem.* **2004**, *69* (21), 6967–6973.

(27) Sadezky, A.; Winterhalter, R.; Kanawati, B.; Rompp, A.; Spengler, B.; Mellouki, A.; Le Bras, G.; Chaimbault, P.; Moortgat, G. K. Oligomer formation during gas-phase ozonolysis of small alkenes and enol ethers: new evidence for the central role of the Criegee Intermediate as oligomer chain unit. *Atmos. Chem. Phys. Discuss.* **2007**, *7*, 14041–14102.

(28) Story, P. R.; Burgess, J. R. Ozonolysis. Evidence for carbonyl oxide tautomerization and for 1,3-dipolar addition to olefins. *J. Am. Chem. Soc.* **1967**, *89* (22), 5726–5727.

(29) Story, P.; Burgess, J. Additions and Corrections - Ozonolysis. Evidence for Carbonyl Oxide Tautomerization and for 1,3-Dipolar Addition to Olefins. *J. Am. Chem. Soc.* **1968**, *90* (4), 1094–1094.

(30) Kroll, J. H.; Sahay, S. R.; Anderson, J. G.; Demerjian, K. L.; Donahue, N. M. Mechanism of HOx formation in the gas-phase ozone-alkene reaction. 2. Prompt versus thermal dissociation of carbonyl oxides to form OH. *J. Phys. Chem. A* **2001**, *105* (18), 4446–4457.

(31) Presto, A. A.; Donahue, N. M. Ozonolysis Fragment Quenching by Nitrate Formation: The Pressure Dependence of Prompt OH Radical Formation. *J. Phys. Chem. A* **2004**, *108*, 9096–9104.

(32) Paulson, S.; Orlando, J. The Reactions of Ozone with Alkenes: An Important Source of HOx in the Boundary Layer. *J. Geophys. Res. Lett.* **1996**, *23*, 3727.

(33) Gutbrod, R.; Schindler, R. N.; Kraka, E.; Cremer, D. Formation of OH radicals in the gas phase ozonolysis of alkenes: the unexpected role of carbonyl oxides. *Chem. Phys. Lett.* **1996**, *252* (3−4), 221–229.

(34) Murray, R. W.; Agarwal, S. K. Ozonolysis of some tetrasubstituted ethylenes. *J. Org. Chem.* **1985**, *50* (24), 4698–4702.

(35) Criegee, R.; Korber, H. Preparation of Some Simple Ketozonides. *Chem. Ber.-Recl.* **1971**, *104* (6), 1812–&.

(36) Griesbaum, K.; Volpp, W.; Greinert, R. Ozonolysis of olefins adsorbed on polyethylene: a new access to ozonides by cycloadditions of carbonyl oxides to ketones. *J. Am. Chem. Soc.* **1985**, *107* (18), 5309–5310.

(37) Aronovitch, C.; Tal, D.; Mazur, Y. Ozonolysis of olfefins and acetylenes adsorbed on silica gel. *Tetrahedron Lett.* **1982**, *23* (35), 3623–3626.

(38) Fong, G. D.; Kuczkowski, R. L. Mechanism of the ozonolysis of ethylene in the liquid phase. *J. Am. Chem. Soc.* **1980**, *102* (14), 4763–4768.

(39) Lorencak, P.; Kuczkowski, R. L. Microwave spectrum and structure of 2,3,7-trioxabicyclo[2.2.1]hept-5-ene. *J. Phys. Chem.* **1989**, *93* (6), 2276–2279.

(40) Durham, L. J.; Greenwood, F. L. Ozonolysis. X. Molozonide as an intermediate in the ozonolysis of cis- and trans-alkenes. *J. Org. Chem.* **1968**, *33* (4), 1629–1632.

(41) Nelander, B.; Nord, L. Do ozone-olefin complexes really exist. *J. Am. Chem. Soc.* **1979**, *101* (14), 3769–3770.

(42) Kohlmiller, C. K.; Andrews, L. Infrared Spectrum of the Primary Ozonide of Ethylene in Solid Xenon. *J. Am. Chem. Soc.* **1981**, *103*, 2578–2583.

(43) Mile, B.; Morris, G. Infrared spectra and kinetics of decomposition of primary ozonides in the liquid phase at low temperatures. *J. Chem. Soc,. Perkin Trans. 2* **1979**, 1644.

(44) Bariseviciute, R.; Ceponkus, J.; Sablinskas, V. Matrix isolation FTIR spectroscopial study of ethene secondary ozonide. *Central Eur. J. Chem.* **2007**, *5* (1), 71–86.

(45) Kuehne, H.; Guenthard, H. H. Spectroscopic study of the ozone-ethylene reaction. Matrix-infrared spectra of three isotopic ethylene ozonides. *J. Phys. Chem.* **1976**, *80* (11), 1238–1247.

(46) Boelens, H. F. M.; Dijkstra, R. J.; Eilers, P. H. C.; Fitzpatrick, F.; Westerhuis, J. A. New background correction method for liquid chromatography with diode array detection, infrared spectroscopic detection and Raman spectroscopic detection. *J. Chromatogr. A* **2004**, *1057* (1−2), 21–30.

(47) Griffiths, P. R.; Haseth, J. A. *Fourier Transform Infrared Spectrometry*; John Wiley & Sons, Inc.: New York, 1986; Vol. 83.

(48) Redhead, P. A. Thermal Desorption of Gases. *Vacuum* **1962**, 203–211.

(49) Frisch, M. J.; Trucks, G. W.; Schlegel, H. B.; Scuseria, G. E.; Robb, M. A.; Cheeseman, J. R. ; Montgomery, J. A., Jr.; Vreven, T.; Kudin, K. N.; Burant, J. C.; Millam, J. M.; Iyengar, S. S.; Tomasi, J.; Barone, V.; Mennucci, B.; Cossi, M.; Scalmani, G.; Rega, N.; Petersson, G. A.; Nakatsuji, H.; Hada, M.; Ehara, M.; Toyota, K.; Fukuda, R.; Hasegawa, J.; Ishida, M.; Nakajima, T.; Honda, Y.; Kitao, O.; Nakai, H.; Klene, M.; Li, X.; Knox, J. E.; Hratchian, H. P.; Cross, J. B.; Bakken, V.; Adamo, C.; Jaramillo, J.; Gomperts, R.; Stratmann, R. E.; Yazyev, O.; Austin, A. J.; Cammi, R.; Pomelli, C.; Ochterski, J. W.; Ayala, P. Y.; Morokuma, K.; Voth, G. A.; Salvador, P.; Dannenberg, J. J.; Zakrzewski, V. G.; Dapprich, S.; Daniels, A. D.; Strain, M. C.; Farkas, O.; Malick, D. K.; Rabuck, A. D.; Raghavachari, K.; Foresman, J. B.; Ortiz, J. V.; Cui, Q.; Baboul, A. G.; Clifford, S.; Cioslowski, J.; Stefanov, B. B.; Liu, G.; Liashenko, A.; Piskorz, P.; Komaromi, I.; Martin, R. L.; Fox, D. J.; Keith, T.; Al-Laham, M. A.; Peng, C. Y.; Nanayakkara, A.; Challacombe, M.; Gill, P. M. W.; Johnson, B.; Chen, W.; Wong, M. W.; Gonzalez, C.; Pople, J. A. Gaussian, Inc.: Wallingford, CT, 2004.

(50) Baer, T.; Hase, W. *Unimolecular Reaction Dynamics: Theory and Experiments*; Oxford University Press: New York, 1996.

(51) Chuong, B.; Zhang, J.; Donahue, N. M. Cycloalkene Ozonolysis: Collisionally Mediated Mechanistic Branching. *J. Am. Chem. Soc.* **2004**, *126* (39), 12363–12373.

(52) Wong, M. W. Vibrational frequency prediction using density functional theory. *Chem. Phys. Lett.* **1996**, *256* (4−5), 391–399.

(53) Hair, M. *Infrared Spectroscopy in Surface Chemistry*; Marcel Dekker, Inc.: New York, 1967.

(54) Atkinson, R.; Aschmann, S. Hydroxyl radical production from the gas-phase reactions of ozone with a series of alkenes under atmospheric conditions. *Environ. Sci. Technol.* **1993**, *27* (7), 1357–1363.

(55) Gutbrod, R.; Rahmann, M.; Schindler, R. *Air Pollut. Res. Rep.* **1994**, *54*, 133.

(56) Anglada, J. M.; Bofill, J. M.; Olivella, S.; Sole, A. Unimolecular Isomerizations and Oxygen Atom Loss in Formaldehyde and Acetaldehyde Carbonyl Oxides. A Theoretical Investigation. *J. Am. Chem. Soc.* **1996**, *118* (19), 4636–4647.

(57) Peng, C.; Schlegel, H. B. Combining Synchronous Transit and Quasi-Newton Methods to Find Transition States. *Israel J. Chem.* **1993**, *33*, 449.

JP807682Y